Measurement of the $D^*(2010)^+$ Natural Line Width and the $D^*(2010)^+ - D^0$ Mass Difference

J. P. Lees, V. Poireau, and V. Tisserand
Laboratoire d'Annecy-le-Vieux de Physique des Particules (LAPP),
Université de Savoie, CNRS/IN2P3, F-74941 Annecy-Le-Vieux, France

E. Grauges
Universitat de Barcelona, Facultat de Fisica, Departament ECM, E-08028 Barcelona, Spain

A. Palano[ab]
INFN Sezione di Bari[a]; Dipartimento di Fisica, Università di Bari[b], I-70126 Bari, Italy

G. Eigen and B. Stugu
University of Bergen, Institute of Physics, N-5007 Bergen, Norway

D. N. Brown, L. T. Kerth, Yu. G. Kolomensky, and G. Lynch
Lawrence Berkeley National Laboratory and University of California, Berkeley, California 94720, USA

H. Koch and T. Schroeder
Ruhr Universität Bochum, Institut für Experimentalphysik 1, D-44780 Bochum, Germany

C. Hearty, T. S. Mattison, J. A. McKenna, and R. Y. So
University of British Columbia, Vancouver, British Columbia, Canada V6T 1Z1

A. Khan
Brunel University, Uxbridge, Middlesex UB8 3PH, United Kingdom

V. E. Blinov, A. R. Buzykaev, V. P. Druzhinin, V. B. Golubev, E. A. Kravchenko, A. P. Onuchin,
S. I. Serednyakov, Yu. I. Skovpen, E. P. Solodov, K. Yu. Todyshev, and A. N. Yushkov
Budker Institute of Nuclear Physics SB RAS, Novosibirsk 630090, Russia

D. Kirkby, A. J. Lankford, and M. Mandelkern
University of California at Irvine, Irvine, California 92697, USA

B. Dey, J. W. Gary, O. Long, and G. M. Vitug
University of California at Riverside, Riverside, California 92521, USA

C. Campagnari, M. Franco Sevilla, T. M. Hong, D. Kovalskyi, J. D. Richman, and C. A. West
University of California at Santa Barbara, Santa Barbara, California 93106, USA

A. M. Eisner, W. S. Lockman, A. J. Martinez, B. A. Schumm, and A. Seiden
University of California at Santa Cruz, Institute for Particle Physics, Santa Cruz, California 95064, USA

D. S. Chao, C. H. Cheng, B. Echenard, K. T. Flood, D. G. Hitlin, P. Ongmongkolkul, and F. C. Porter
California Institute of Technology, Pasadena, California 91125, USA

R. Andreassen, C. Fabby, Z. Huard, B. T. Meadows, M. D. Sokoloff, and L. Sun
University of Cincinnati, Cincinnati, Ohio 45221, USA

P. C. Bloom, W. T. Ford, A. Gaz, U. Nauenberg, J. G. Smith, and S. R. Wagner
University of Colorado, Boulder, Colorado 80309, USA

R. Ayad[*] and W. H. Toki

Colorado State University, Fort Collins, Colorado 80523, USA

B. Spaan

Technische Universität Dortmund, Fakultät Physik, D-44221 Dortmund, Germany

K. R. Schubert and R. Schwierz

Technische Universität Dresden, Institut für Kern- und Teilchenphysik, D-01062 Dresden, Germany

D. Bernard and M. Verderi

Laboratoire Leprince-Ringuet, Ecole Polytechnique, CNRS/IN2P3, F-91128 Palaiseau, France

S. Playfer

University of Edinburgh, Edinburgh EH9 3JZ, United Kingdom

D. Bettoni[a], C. Bozzi[a], R. Calabrese[ab], G. Cibinetto[ab], E. Fioravanti[ab],
I. Garzia[ab], E. Luppi[ab], L. Piemontese[a], and V. Santoro[a]

INFN Sezione di Ferrara[a]; Dipartimento di Fisica, Università di Ferrara[b], I-44100 Ferrara, Italy

R. Baldini-Ferroli, A. Calcaterra, R. de Sangro, G. Finocchiaro,
P. Patteri, I. M. Peruzzi,[†] M. Piccolo, M. Rama, and A. Zallo

INFN Laboratori Nazionali di Frascati, I-00044 Frascati, Italy

R. Contri[ab], E. Guido[ab], M. Lo Vetere[ab], M. R. Monge[ab], S. Passaggio[a], C. Patrignani[ab], and E. Robutti[a]

INFN Sezione di Genova[a]; Dipartimento di Fisica, Università di Genova[b], I-16146 Genova, Italy

B. Bhuyan and V. Prasad

Indian Institute of Technology Guwahati, Guwahati, Assam, 781 039, India

M. Morii

Harvard University, Cambridge, Massachusetts 02138, USA

A. Adametz and U. Uwer

Universität Heidelberg, Physikalisches Institut, Philosophenweg 12, D-69120 Heidelberg, Germany

H. M. Lacker

Humboldt-Universität zu Berlin, Institut für Physik, Newtonstr. 15, D-12489 Berlin, Germany

P. D. Dauncey

Imperial College London, London, SW7 2AZ, United Kingdom

U. Mallik

University of Iowa, Iowa City, Iowa 52242, USA

C. Chen, J. Cochran, W. T. Meyer, S. Prell, and A. E. Rubin

Iowa State University, Ames, Iowa 50011-3160, USA

A. V. Gritsan

Johns Hopkins University, Baltimore, Maryland 21218, USA

N. Arnaud, M. Davier, D. Derkach, G. Grosdidier, F. Le Diberder,
A. M. Lutz, B. Malaescu, P. Roudeau, A. Stocchi, and G. Wormser

*Laboratoire de l'Accélérateur Linéaire, IN2P3/CNRS et Université Paris-Sud 11,
Centre Scientifique d'Orsay, B. P. 34, F-91898 Orsay Cedex, France*

D. J. Lange and D. M. Wright

Lawrence Livermore National Laboratory, Livermore, California 94550, USA

J. P. Coleman, J. R. Fry, E. Gabathuler, D. E. Hutchcroft, D. J. Payne, and C. Touramanis
University of Liverpool, Liverpool L69 7ZE, United Kingdom

A. J. Bevan, F. Di Lodovico, R. Sacco, and M. Sigamani
Queen Mary, University of London, London, E1 4NS, United Kingdom

G. Cowan
University of London, Royal Holloway and Bedford New College, Egham, Surrey TW20 0EX, United Kingdom

J. Bougher, D. N. Brown, and C. L. Davis
University of Louisville, Louisville, Kentucky 40292, USA

A. G. Denig, M. Fritsch, W. Gradl, K. Griessinger, A. Hafner, and E. Prencipe
Johannes Gutenberg-Universität Mainz, Institut für Kernphysik, D-55099 Mainz, Germany

R. J. Barlow[‡] and G. D. Lafferty
University of Manchester, Manchester M13 9PL, United Kingdom

E. Behn, R. Cenci, B. Hamilton, A. Jawahery, and D. A. Roberts
University of Maryland, College Park, Maryland 20742, USA

R. Cowan, D. Dujmic, and G. Sciolla
Massachusetts Institute of Technology, Laboratory for Nuclear Science, Cambridge, Massachusetts 02139, USA

R. Cheaib, P. M. Patel,[§] and S. H. Robertson
McGill University, Montréal, Québec, Canada H3A 2T8

P. Biassoni[ab], N. Neri[a], and F. Palombo[ab]
INFN Sezione di Milano[a]; Dipartimento di Fisica, Università di Milano[b], I-20133 Milano, Italy

L. Cremaldi, R. Godang,[¶] P. Sonnek, and D. J. Summers
University of Mississippi, University, Mississippi 38677, USA

X. Nguyen, M. Simard, and P. Taras
Université de Montréal, Physique des Particules, Montréal, Québec, Canada H3C 3J7

G. De Nardo[ab], D. Monorchio[ab], G. Onorato[ab], and C. Sciacca[ab]
INFN Sezione di Napoli[a]; Dipartimento di Scienze Fisiche,
Università di Napoli Federico II[b], I-80126 Napoli, Italy

M. Martinelli and G. Raven
NIKHEF, National Institute for Nuclear Physics and High Energy Physics, NL-1009 DB Amsterdam, The Netherlands

C. P. Jessop and J. M. LoSecco
University of Notre Dame, Notre Dame, Indiana 46556, USA

K. Honscheid and R. Kass
Ohio State University, Columbus, Ohio 43210, USA

J. Brau, R. Frey, N. B. Sinev, D. Strom, and E. Torrence
University of Oregon, Eugene, Oregon 97403, USA

E. Feltresi[ab], N. Gagliardi[ab], M. Margoni[ab], M. Morandin[a],
M. Posocco[a], M. Rotondo[a], G. Simi[a], F. Simonetto[ab], and R. Stroili[ab]
INFN Sezione di Padova[a]; Dipartimento di Fisica, Università di Padova[b], I-35131 Padova, Italy

S. Akar, E. Ben-Haim, M. Bomben, G. R. Bonneaud, H. Briand,

G. Calderini, J. Chauveau, Ph. Leruste, G. Marchiori, J. Ocariz, and S. Sitt

Laboratoire de Physique Nucléaire et de Hautes Energies,
IN2P3/CNRS, Université Pierre et Marie Curie-Paris6,
Université Denis Diderot-Paris7, F-75252 Paris, France

M. Biasini[ab], E. Manoni[ab], S. Pacetti[ab], and A. Rossi[ab]

INFN Sezione di Perugia[a]; Dipartimento di Fisica, Università di Perugia[b], I-06100 Perugia, Italy

C. Angelini[ab], G. Batignani[ab], S. Bettarini[ab], M. Carpinelli[ab],[**] G. Casarosa[ab], A. Cervelli[ab], F. Forti[ab],
M. A. Giorgi[ab], A. Lusiani[ac], B. Oberhof[ab], E. Paoloni[ab], A. Perez[a], G. Rizzo[ab], and J. J. Walsh[a]

INFN Sezione di Pisa[a]; Dipartimento di Fisica, Università di Pisa[b]; Scuola Normale Superiore di Pisa[c], I-56127 Pisa, Italy

D. Lopes Pegna, J. Olsen, and A. J. S. Smith

Princeton University, Princeton, New Jersey 08544, USA

F. Anulli[a], R. Faccini[ab], F. Ferrarotto[a], F. Ferroni[ab], M. Gaspero[ab], L. Li Gioi[a], and G. Piredda[a]

INFN Sezione di Roma[a]; Dipartimento di Fisica,
Università di Roma La Sapienza[b], I-00185 Roma, Italy

C. Bünger, O. Grünberg, T. Hartmann, T. Leddig, C. Voß, and R. Waldi

Universität Rostock, D-18051 Rostock, Germany

T. Adye, E. O. Olaiya, and F. F. Wilson

Rutherford Appleton Laboratory, Chilton, Didcot, Oxon, OX11 0QX, United Kingdom

S. Emery, G. Hamel de Monchenault, G. Vasseur, and Ch. Yèche

CEA, Irfu, SPP, Centre de Saclay, F-91191 Gif-sur-Yvette, France

D. Aston, D. J. Bard, J. F. Benitez, C. Cartaro, M. R. Convery, J. Dorfan, G. P. Dubois-Felsmann,
W. Dunwoodie, M. Ebert, R. C. Field, B. G. Fulsom, A. M. Gabareen, M. T. Graham, C. Hast,
W. R. Innes, P. Kim, M. L. Kocian, D. W. G. S. Leith, P. Lewis, D. Lindemann, B. Lindquist, S. Luitz,
V. Luth, H. L. Lynch, D. B. MacFarlane, D. R. Muller, H. Neal, S. Nelson, M. Perl, T. Pulliam,
B. N. Ratcliff, A. Roodman, A. A. Salnikov, R. H. Schindler, A. Snyder, D. Su, M. K. Sullivan, J. Va'vra,
A. P. Wagner, W. F. Wang, W. J. Wisniewski, M. Wittgen, D. H. Wright, H. W. Wulsin, and V. Ziegler

SLAC National Accelerator Laboratory, Stanford, California 94309 USA

W. Park, M. V. Purohit, R. M. White, and J. R. Wilson

University of South Carolina, Columbia, South Carolina 29208, USA

A. Randle-Conde and S. J. Sekula

Southern Methodist University, Dallas, Texas 75275, USA

M. Bellis, P. R. Burchat, T. S. Miyashita, and E. M. T. Puccio

Stanford University, Stanford, California 94305-4060, USA

M. S. Alam and J. A. Ernst

State University of New York, Albany, New York 12222, USA

R. Gorodeisky, N. Guttman, D. R. Peimer, and A. Soffer

Tel Aviv University, School of Physics and Astronomy, Tel Aviv, 69978, Israel

S. M. Spanier

University of Tennessee, Knoxville, Tennessee 37996, USA

J. L. Ritchie, A. M. Ruland, R. F. Schwitters, and B. C. Wray

University of Texas at Austin, Austin, Texas 78712, USA

J. M. Izen and X. C. Lou
University of Texas at Dallas, Richardson, Texas 75083, USA

F. Bianchi[ab], D. Gamba[ab], and S. Zambito[ab]
INFN Sezione di Torino[a]; Dipartimento di Fisica Sperimentale, Università di Torino[b], I-10125 Torino, Italy

L. Lanceri[ab] and L. Vitale[ab]
INFN Sezione di Trieste[a]; Dipartimento di Fisica, Università di Trieste[b], I-34127 Trieste, Italy

F. Martinez-Vidal, A. Oyanguren, and P. Villanueva-Perez
IFIC, Universitat de Valencia-CSIC, E-46071 Valencia, Spain

H. Ahmed, J. Albert, Sw. Banerjee, F. U. Bernlochner, H. H. F. Choi, G. J. King, R. Kowalewski,
M. J. Lewczuk, T. Lueck, I. M. Nugent, J. M. Roney, R. J. Sobie, and N. Tasneem
University of Victoria, Victoria, British Columbia, Canada V8W 3P6

T. J. Gershon, P. F. Harrison, and T. E. Latham
Department of Physics, University of Warwick, Coventry CV4 7AL, United Kingdom

H. R. Band, S. Dasu, Y. Pan, R. Prepost, and S. L. Wu
University of Wisconsin, Madison, Wisconsin 53706, USA

(The *BABAR* Collaboration)

We measure the mass difference, Δm_0, between the $D^*(2010)^+$ and the D^0 and the natural line width, Γ, of the transition $D^*(2010)^+ \to D^0\pi^+$. The data were recorded with the *BABAR* detector at center-of-mass energies at and near the $\Upsilon(4S)$ resonance, and correspond to an integrated luminosity of approximately $477\,\text{fb}^{-1}$. The D^0 is reconstructed in the decay modes $D^0 \to K^-\pi^+$ and $D^0 \to K^-\pi^+\pi^-\pi^+$. For the decay mode $D^0 \to K^-\pi^+$ we obtain $\Gamma = (83.4 \pm 1.7 \pm 1.5)$ keV and $\Delta m_0 = (145\,425.6 \pm 0.6 \pm 1.8)$ keV, where the quoted errors are statistical and systematic, respectively. For the $D^0 \to K^-\pi^+\pi^-\pi^+$ mode we obtain $\Gamma = (83.2 \pm 1.5 \pm 2.6)$ keV and $\Delta m_0 = (145\,426.6 \pm 0.5 \pm 2.0)$ keV. The combined measurements yield $\Gamma = (83.3 \pm 1.3 \pm 1.4)$ keV and $\Delta m_0 = (145\,425.8 \pm 0.5 \pm 1.8)$ keV; the width is a factor of approximately 12 times more precise than the best previous value, while the mass difference is a factor of approximately 6 times more precise.

PACS numbers: 13.20.Fc, 13.25.Ft, 14.40.Lb, 12.38.Gc, 12.38.Qk, 12.39.Ki, 12.39.Pn

INTRODUCTION

The $D^*(2010)^+$ (D^{*+}) line width provides a window into a nonperturbative regime of strong physics where the charm quark is the heaviest meson constituent [1–3]. The line width provides an experimental check of models of the D meson spectrum, and is related to the strong coupling of the D^{*+} to the $D\pi$ system, $g_{D^*D\pi}$. In the heavy-quark limit, which is not necessarily a good approximation for the charm quark [4], this coupling can be related to the universal coupling of heavy mesons to a pion, $\hat{g}$. There is no direct experimental window on the corresponding coupling in the B system, $g_{B^*B\pi}$, since there is no phase space for the decay $B^* \to B\pi$. However, the D and B systems can be related through $\hat{g}$, which allows the calculation of $g_{B^*B\pi}$. The $B^*B\pi$ coupling is needed for a model-independent extraction of $|V_{ub}|$ [5, 6] and is presently one of the largest contributions to the theoretical uncertainty on $|V_{ub}|$ [7].

We study the $D^{*+} \to D^0\pi^+$ transition using the $D^0 \to$ $K^-\pi^+$ and $D^0 \to K^-\pi^+\pi^-\pi^+$ decay modes to measure the values of the D^{*+} line width, Γ, and the difference between the D^{*+} and D^0 masses, Δm_0 [8]. The best prior measurement of the width is $\Gamma = (96 \pm 4 \pm 22)$ keV by the CLEO collaboration where the uncertainties are statistical and systematic, respectively [9]. That measurement is based on a data sample corresponding to an integrated luminosity of $9\,\text{fb}^{-1}$ and reconstructed $D^0 \to K^-\pi^+$ decays. In the present analysis, we have a data sample that is approximately 50 times larger. This allows us to apply tight selection criteria to reduce background, and to investigate sources of systematic uncertainty with high precision.

The signal is described by a relativistic Breit-Wigner (RBW) function defined by

$$\frac{d\Gamma(m)}{dm} = \frac{m\Gamma_{D^*D\pi}(m)\,m_0\Gamma}{(m_0^2 - m^2)^2 + (m_0\Gamma_{\text{Total}}(m))^2}, \quad (1)$$

where $\Gamma_{D^*D\pi}$ is the partial width to $D^0\pi^+$, m is the $D^0\pi^+$ invariant mass, m_0 is the invariant mass at the

pole, and $\Gamma_{\text{Total}}(m)$ is the total D^{*+} decay width. The partial width is defined by

$$\Gamma_{D^*D\pi}(m) = \Gamma \left(\frac{\mathcal{F}^\ell_{D\pi}(p_0)}{\mathcal{F}^\ell_{D\pi}(p)} \right)^2 \left(\frac{p}{p_0} \right)^{2\ell+1} \left(\frac{m_0}{m} \right), \quad (2)$$

where $\mathcal{F}^{\ell=1}_{D\pi}(p) = \sqrt{1 + r^2 p^2}$ is the Blatt-Weisskopf form factor for a vector particle with radius parameter r and daughter momentum p, and the subscript zero denotes a quantity measured at the pole [10, 11]. The value of the radius is unknown, but for the charm sector it is expected to be $\sim 1\,\text{GeV}^{-1}$ [12]. We use the value $r = 1.6\,\text{GeV}^{-1}$ from Ref. [13] and vary this value as part of our investigation of systematic uncertainties.

Key to this analysis is that the tails of the RBW are much longer than the almost Gaussian resolution function, which allows us to use information far from the central signal region to measure the width.

This paper is organized as follows. Section discusses the *BABAR* detector and the data used in this analysis, and Section describes the event selection. Section discusses a correction to the detector material model and magnetic field map. Section details the fit strategy, Section discusses and quantifies the sources of systematic uncertainty, and Section describes how the results for the two D^0 decay modes are combined to obtain the final results. Finally, the results are summarized in Section .

THE *BABAR* DETECTOR AND DATA

This analysis is based on a data sample corresponding to an integrated luminosity of approximately $477\,\text{fb}^{-1}$ recorded at and 40 MeV below the $\Upsilon(4S)$ resonance by the *BABAR* detector at the PEP-II asymmetric energy e^+e^- collider. The *BABAR* detector is described in detail elsewhere [14], so we summarize only the relevant components below. Charged particles are measured with a combination of a 40-layer cylindrical drift chamber (DCH) and a 5-layer double-sided silicon vertex tracker (SVT), both operating within the 1.5-T magnetic field of a superconducting solenoid. Information from a ring-imaging Cherenkov detector is combined with specific ionization (dE/dx) measurements from the SVT and DCH to identify charged kaon and pion candidates. Electrons are identified, and photons measured, with a CsI(Tl) electromagnetic calorimeter. The return yoke of the superconducting coil is instrumented with tracking chambers for the identification of muons.

EVENT SELECTION

We reconstruct continuum-produced $D^{*+} \to D^0 \pi_s^+$ decays in the two Cabibbo-favored channels $D^0 \to K^-\pi^+$ and $D^0 \to K^-\pi^+\pi^-\pi^+$. The pion from the D^{*+} decay is called the "slow pion" (denoted π_s^+) because of the limited phase space available. The selection criteria for the individual D^0 channels are detailed below; however, both modes have the same D^{*+} requirements. The selection criteria were chosen to enhance the signal-to-background ratio (S/B) to increase the sensitivity to the long RBW tails in the Δm distribution; we have not optimized the criteria for statistical significance. Because this analysis depends on the RBW tails, we pay particular attention to how the selection criteria affect the tail regions.

The entire decay chain is fit using a kinematic fitter with geometric constraints at each vertex, and the additional constraint that the D^{*+} candidates originate from the interaction region. The confidence level of the χ^2 of the fit to the entire decay chain is required to be at least 0.1%. If there is more than one D^{*+} candidate in the event, we choose the one with the highest confidence level. The mass difference between the D^{*+} and D^0 is required to satisfy $\Delta m < 0.17\,\text{GeV}$. A large amount of the combinatorial and B meson decay background is removed by requiring $p^*(D^{*+}) > 3.6\,\text{GeV}$, where p^* is the momentum measured in the e^+e^- center-of-mass frame for the event. Selecting Cabibbo-favored decay modes avoids a large amount of combinatorial background mimicking signal from doubly Cabibbo-suppressed decays.

The experimental uncertainty in the measured invariant mass difference is dominated by the uncertainty on the measured momentum of the slow pion. Therefore, we choose criteria to select well-measured pions. For improved tracking resolution we require that the π_s^+ tracks have at least 12 measurements in the DCH and have at least 6 SVT measurements with at least 2 in the first three layers. We reduce backgrounds from other species of tracks in our slow pion sample by requiring that the dE/dx values reported by the SVT and DCH be consistent with the pion hypothesis.

The Dalitz decay $\pi^0 \to \gamma e^+e^-$ results in a problematic background where we misidentify an electron as a π_s^+. We eliminate such candidates by reconstructing a candidate e^+e^- pair and combining it with a γ. If the e^+e^- vertex is within the SVT volume and the invariant mass is in the range $115\,\text{MeV} < m\,(\gamma e^+e^-) < 155\,\text{MeV}$, then the event is rejected. Photon conversions in the detector material are another source of background where electrons can be misidentified as slow pions. To identify such conversions we first create a candidate e^+e^- pair using the slow pion candidate and an identified electron track from the same event and perform a least-squares fit with a geometric constraint. The event is rejected if the invariant mass of the putative pair is less than 60 MeV and the constrained vertex position is within the SVT tracking volume.

We identified additional criteria to remove candidates in kinematic regions where the Monte Carlo (MC) simulation poorly models the data. The MC is a cocktail of $q\bar{q}$ and $\ell^+\ell^-$ sources where $q = u,d,s,c,b$ and

$\ell = e, \mu, \tau$. The simulation does not accurately replicate the momentum distributions observed in data at very high and low D^{*+} momentum values, so we require that $3.6\,\text{GeV} < p^*(D^{*+}) < 4.3\,\text{GeV}$ and that the laboratory momentum of the slow pion be at least 150 MeV. In an independent sample of $K_S^0 \to \pi^-\pi^+$ decays, the reconstructed K_S^0 mass is observed to vary as a function of the polar angle θ of the K_S^0 momentum measured in the laboratory frame with respect to the electron beam axis. We define the acceptance angle to reject events where any of the daughter tracks of the D^{*+} has $\cos\theta \geq 0.89$ to exclude the very-forward region of the detector. This criterion reduces the final data samples by approximately 10%.

For both $D^0 \to K^-\pi^+$ and $D^0 \to K^-\pi^+\pi^-\pi^+$, we apply particle identification (PID) requirements to the K and π candidate tracks. To select candidates with better tracking resolution, and consequently improve the resolution of the reconstructed masses, we require that D^0 daughter tracks have at least 21 measurements in the DCH and satisfy the same SVT measurement requirements as the slow pion track described before. The reconstructed D^0 mass must be within the range 1.86 GeV to 1.87 GeV, and the confidence level of the χ^2 of the fit of the D^0 with kinematic and geometric constraints must be at least 0.5%.

The background level in the $D^0 \to K^-\pi^+\pi^-\pi^+$ mode is much higher than that in $D^0 \to K^-\pi^+$, and so we require D^0 daughter charged tracks to satisfy stricter PID requirements. The higher background arises because the D^0 mass is on the tail of two-body $K^-\pi^+$ invariant mass distribution expected in a longitudinal phase space model, however it is near the peak of the 4-body $K^-\pi^+\pi^-\pi^+$ invariant mass distribution [15]. Compounding this phase space effect is the greater probability of wrongly assigning a track while still mimicking a correctly reconstructed D^0.

The initial fit to the $D^0 \to K^-\pi^+\pi^-\pi^+$ validation signal MC sample had a bias in the measured value of the D^{*+} width. An extensive comparison revealed that the bias originated from regions of phase space that the MC generator populated more frequently than the data. Evidently, there are amplitudes that suppress these structures in the data, that are neither known nor included in the MC generator. We avoid the regions where the MC disagrees with the data by rejecting a candidate if either $\left(m^2\left(\pi^+\pi^+\right) < -1.17\,m^2\left(\pi^-\pi^+\right) + 0.46\,\text{GeV}^2\right)$ or $\left(m^2\left(\pi^-\pi^+\right) < 0.35\,\text{GeV}^2 \text{ and } m^2\left(K^-\pi^+\right) < 0.6\,\text{GeV}^2\right)$. This veto is applied for each π^+ daughter of the D^0 candidate.

There is an additional source of background that must be taken into account for the $K^-\pi^+\pi^-\pi^+$ channel that is negligible for the $K^-\pi^+$ channel. In a small fraction of events ($< 1\%$) we mistakenly exchange the slow pion from D^{*+} decay with one of the same-sign D^0 daughter pions. This shifts the reconstructed mass values and in-

troduces a $\mathcal{O}(0.1\,\text{keV})$ bias on the width obtained from the fits to the validation signal MC sample. To veto these events we recalculate the invariant mass values after intentionally switching the same-sign pions, and create the variable $\Delta m' \equiv m\left(K^-\pi^+\pi^-\pi^+\pi_s^+\right) - m\left(K^-\pi^+\pi^-\pi_s^+\right)$. There are two pions from the D^0 decay with the same charge as the slow pion, so there are two values of $\Delta m'$ to consider. In this procedure the correctly reconstructed events are moved away from the signal region, while events with this mis-reconstruction are shifted into the signal region. We reject events with $\Delta m' < 0.1665\,\text{GeV}$. Using fits to the validation signal MC sample we found that by using this criterion rather than using a narrow range, we are able to remove approximately 80% of the misreconstructed events and this removes the bias of the fitted value of the width.

MATERIAL MODELING

In the initial fits to data, we observed a very strong dependence of the RBW pole position on the slow pion momentum. This dependence is not replicated in the MC, and originates in the magnetic field map and in the modeling of the material of the beam pipe and the SVT. Previous BABAR analyses have observed such effects. For example, in the measurement of the Λ_c^+ mass [16] the material model of the SVT was altered in an attempt to correct for the energy loss and the under-represented small-angle multiple scattering (due to nuclear Coulomb scattering). However, the momentum dependence could be removed only by adding an unphysical amount of material to the SVT. The corrections described here avoid altering the underlying detector model and focus on adjusting track momenta after reconstruction.

We use a sample of $K_S^0 \to \pi^+\pi^-$ candidates from $D^{*+} \to D^0\pi^+$ decay, where we reconstruct $D^0 \to K_S^0\pi^-\pi^+$, and require that the K_S^0 daughter pions satisfy the same tracking criteria as the slow pions of the D^{*+} analysis. The K_S^0 decay vertex is required to be inside the beam pipe and to be well-separated from the D^0 decay vertex. These selection criteria yield an extremely clean K_S^0 sample ($> 99.5\%$ pure), which is used to determine fractional corrections to the overall magnetic field and to the energy losses in the beam pipe (E_loss^bmp) and, separately, in the SVT (E_loss^svt). The points represented as open squares in Fig. 1 show the strong dependence of the reconstructed K_S^0 mass on laboratory momentum. Adjusting only the estimated energy losses and detector material flattens the distribution, but there is still a remaining discrepancy. This discrepancy is shown by the open squares in Fig. 1 at high momentum and indicates an overall momentum scale problem. These two effects lead us to consider corrections to the laboratory momentum and energy of an individual track of the form

TABLE I. Energy-loss and momentum correction parameters of Eq. (3) which remove the momentum dependence of the reconstructed K_S^0 mass shown in Fig. 1. The nominal parameters shift the average reconstructed masses to be the PDG mean value, also shown in Fig. 1. To estimate the associated systematic uncertainty, the procedure was repeated to give average reconstructed K_S^0 masses $\pm 1\sigma_{\mathrm{PDG}}$ from the nominal value.

	Nominal	For systematics	
	$m_{\mathrm{PDG}}(K_S^0)$	$m_{\mathrm{PDG}} + 1\sigma_{\mathrm{PDG}}$	$m_{\mathrm{PDG}} - 1\sigma_{\mathrm{PDG}}$
a	0.00030	0.00030	0.00019
b_{bmp}	0.018	0.052	0.030
b_{svt}	0.059	0.059	0.059

$$p \to p\,(1 + a)$$
$$E \to E + b_{\mathrm{bmp}}E_{\mathrm{loss}}^{\mathrm{bmp}} + b_{\mathrm{svt}}E_{\mathrm{loss}}^{\mathrm{svt}} \qquad (3)$$

where the initial energy losses are determined by the Kalman filter based on the material model. We determine the best set of correction parameters to minimize the χ^2 of the bin-by-bin mass difference between the $\pi^+\pi^-$ invariant mass and the current value of the K_S^0 mass ($m_{\mathrm{PDG}}\left(K_S^0\right) \pm 1\sigma_{\mathrm{PDG}} = 497.614 \pm 0.024\,\mathrm{MeV}$) [17].

To assess the systematic uncertainty in values measured from corrected distributions, we find new parameter values by tuning the $\pi^+\pi^-$ invariant mass to the nominal K_S^0 mass shifted up and down by one standard deviation. These three sets of correction parameters are listed in Table I. The corrections corresponding to the nominal K_S^0 mass remove the momentum dependence of $m\left(\pi^+\pi^-\right)$ as illustrated by the points shown as solid dots in Fig. 1.

The best-fit value of $a = 0.00030$ corresponds to an increase of 4.5 Gauss on the central magnetic field. This is larger than the nominal 2 Gauss sensitivity of the magnetic field mapping [14]. However, the azimuthal dependence of Δm_0 (discussed in Sec.) indicates that the accuracy of the mapping may be less than originally thought.

The momentum dependence of Δm_0 in the initial results is ascribed to underestimating the dE/dx loss in the beam pipe and SVT, which we correct using the factors b_{bmp} (1.8%) and b_{SVT} (5.9%). Typical dE/dx losses for a minimum ionizing particle with laboratory momentum $2\,\mathrm{GeV}$ traversing the beam pipe and SVT at normal incidence are $4.4\,\mathrm{MeV}$. The corrections are most significant for low-momentum tracks. However, the corrections are applied to all D^{*+} daughter tracks, not just to the slow pion. The momentum dependence was eliminated after the corrections were applied. All fits to data described in this analysis are performed using masses and Δm values calculated using corrected 4-momenta. The MC tracks
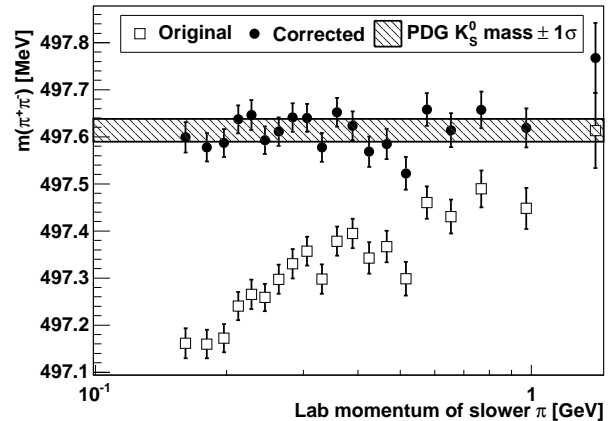

FIG. 1. Mass value of the K_S^0 obtained by fitting the invariant $\pi^+\pi^-$ mass distribution shown as a function of the slower pion laboratory momentum before and after energy-loss and momentum corrections have been applied. Note that the horizontal scale is logarithmic.

are not corrected because the same field and material models used to propagate tracks are used during their reconstruction.

FIT METHOD

To measure Γ we fit the Δm peak (the signal) with a relativistic Breit-Wigner (RBW) function convolved with a resolution function based on a Geant4 MC simulation of the detector response [18]. As in previous analyses [9], we approximate the total D^{*+} decay width $\Gamma_{\mathrm{Total}}(m) \approx \Gamma_{D^*D\pi}(m)$, ignoring the electromagnetic contribution from $D^{*+} \to D^+\gamma$. This approximation has a negligible effect on the measured values as it appears only in the denominator of Eq. (1). For the purpose of fitting the Δm distribution we obtain $d\Gamma(\Delta m)/d\Delta m$ from Eqs. (1) and (2) by making the substitution $m = m(D^0) + \Delta m$, where $m(D^0)$ is the current average mass of the D^0 meson [17].

Our fitting procedure involves two steps. In the first step we model the resolution due to track reconstruction by fitting the Δm distribution for correctly reconstructed MC events using a sum of three Gaussians and a function to describe the non-Gaussian component. The second step uses the resolution shape from the first step and convolves the Gaussian components with a relativistic Breit-Wigner of the form in Eq. (1) to fit the Δm distribution in data, and thus measure Γ and Δm_0. We fit the Δm distribution in data and MC from the kinematic threshold to $\Delta m = 0.1665\,\mathrm{GeV}$ using a binned maximum likelihood fit and an interval width of $50\,\mathrm{keV}$.
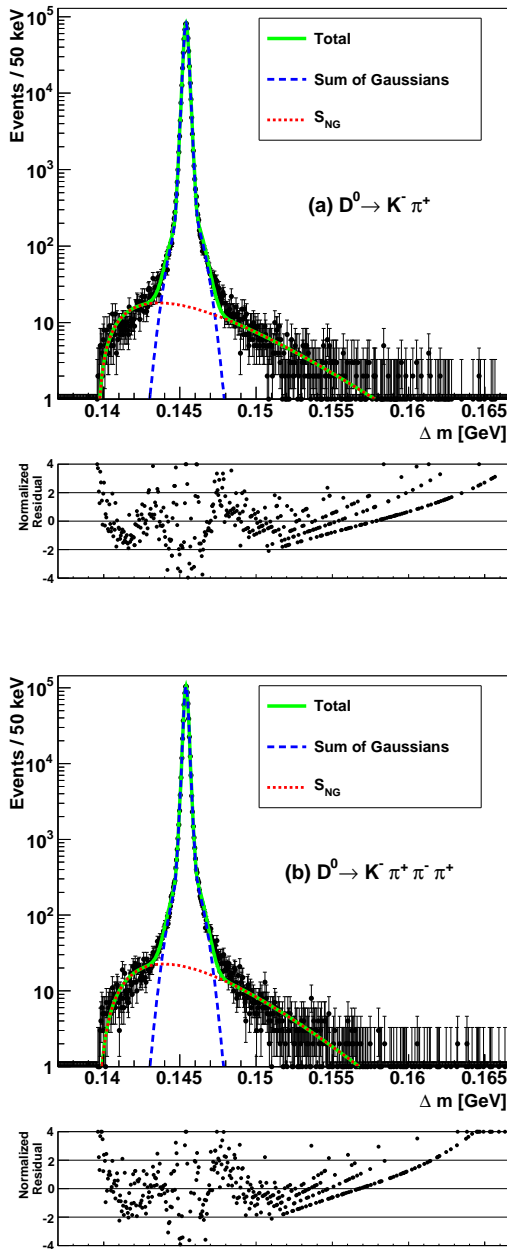
Modeling experimental resolution

FIG. 2. (color online) Binned maximum likelihood fit to the Δm resolution distribution of MC samples for both D^0 decay modes. The interval size is 50 keV, and the high mass tails are dominated by low statistics. Normalized residuals are defined as $(N_{\text{observed}} - N_{\text{predicted}})/\sqrt{N_{\text{predicted}}}$. The shapes in the distribution of the normalized residuals are from dominance by Poisson statistics. In the peak region the total PDF is visually indistinguishable from the Gaussian component of the resolution function.

We generate samples of D^{*+} decays with a line width

of 0.1 keV, so that all of the observed spread is due to reconstruction effects. The non-Gaussian tails of the distribution are from events in which the π_s decays to a μ in flight and where coordinates from both the π and μ segments are used in track reconstruction. Accounting for these non-Gaussian events greatly improves the quality of the fit to data near the Δm peak.

We fit the Δm distribution of the MC events with the function

$$f_{NG}S_{NG}\left(\Delta m; q, \alpha\right) + (1 - f_{NG}^{MC})\left[f_1 G\left(\Delta m; \quad \mu_1, \sigma_1\right)\right.$$
$$\left. + f_2 G\left(\Delta m; \mu_2, \sigma_2\right) + (1 - f_1 - f_2) G\left(\Delta m; \mu_3, \quad \sigma_3\right)\right] \tag{4}$$

where the $G\left(\Delta m; \mu_i, \sigma_i\right)$ are Gaussian functions and f_{NG}, f_1, f_2 are the fractions allotted to the non-Gaussian component and the first and second Gaussian components, respectively. The function describing the non-Gaussian component of the distribution is

$$S_{NG}\left(\Delta m; q, \alpha\right) = \Delta m \, u^q \, e^{\alpha u}, \tag{5}$$

where $u \equiv \left(\Delta m/\Delta m_{\text{thres}}\right)^2 - 1$ and $\Delta m_{\text{thres}} = m_\pi$ is the kinematic threshold for the $D^{*+} \to D^0\pi^+$ process. For $\Delta m < \Delta m_{\text{thres}}$, S_{NG} is defined to be zero.

Figure 2 shows the individual resolution function fits for the two D^0 decay modes. Each plot shows the total resolution probability density function (PDF) as the solid curve, the sum of the Gaussian contributions is represented by the dashed curve, and the S_{NG} function as a dotted curve describing the events in the tails. The resolution functions should peak at the generated value, $\Delta m_0^{MC} = m(D^*(2010)^+) - m(D^0)$ [17]. However, the fitted values of the μ_i differ slightly from Δm_0^{MC}, with the result that the superposition of the three Gaussian functions reaches a maximum at a slightly larger value of Δm. The S_{NG} function is excluded from this calculation as the peak position is not well defined and S_{NG} describes less than 1% of the signal. We take this reconstruction bias as an offset when measuring Δm_0 from data and denote this offset by δm_0. The δm_0 offset is 4.3 keV and 2.8 keV for the $D^0 \to K^-\pi^+$ and $D^0 \to K^-\pi^+\pi^-\pi^+$ modes, respectively. As discussed in Sec. , although the values of δm_0 are larger than the final estimates of the systematic uncertainty for Δm_0, they are required for an unbiased result from fits to the validation signal MC samples. The systematic uncertainty associated with δm_0 is implicitly included when we vary the resolution shape, as discussed in Sec. .

Fit Results

The parameters of the resolution function found in the previous step are used to create a convolved RBW PDF. In the fit to data, S_{NG} has a fixed shape and relative
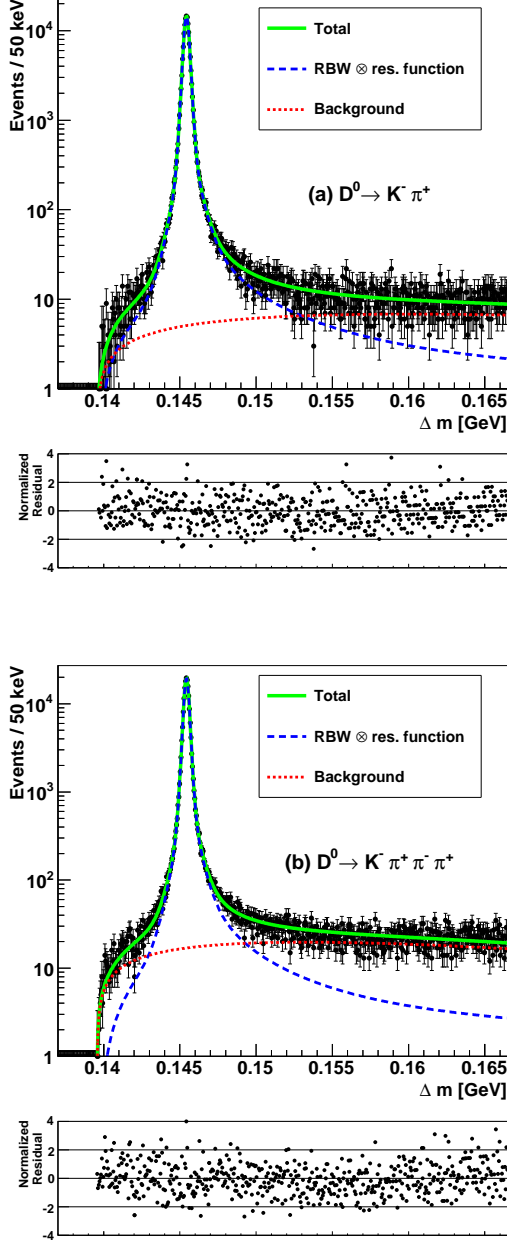
FIG. 3. (color online) The results of the fits to data for each D^0 decay mode. The fitted parameter values are summarized in Table II. The solid curve is the sum of the signal (dashed curve) and background (dotted curve) PDFs. The total PDF and signal component are visually indistinguishable in the peak region.

fraction, and is not convolved with the RBW. The relative contribution of S_{NG} is small and the results from the fits to the validation signal MC samples are unbiased without convolving this term. We fit the data using the function,

$$
\mathcal{P}(\Delta m; \epsilon, \Gamma, \Delta m_0, c) =
$$
$$
f_{\mathcal{S}} \frac{\mathcal{S}(\Delta m; \epsilon, \Gamma, \Delta m_0)}{\int \mathcal{S}(\Delta m)\, d\,(\Delta m)} + (1 - f_{\mathcal{S}}) \frac{\mathcal{B}(\Delta m; c)}{\int \mathcal{B}(\Delta m)\, d\,(\Delta m)} \tag{6}
$$

where $f_{\mathcal{S}}$ is the fraction of signal events, $\mathcal{S}$ is the signal function

$$
\mathcal{S}(\Delta m) = RBW \otimes
$$
$$
(1 - f_{NG}) \left[f_1^{MC} G\left(\Delta m; \mu_1^{MC} - \Delta m_0^{MC}, \sigma_1^{MC}(1 + \epsilon)\right) \right.
$$
$$
+ f_2^{MC}\ G\left(\Delta m; \mu_2^{MC} - \Delta m_0^{MC}, \sigma_2^{MC}(1 + \epsilon)\right)
$$
$$
+ (1 -\ f_1^{MC} - f_2^{MC})
$$
$$
\left. G\left(\Delta m; \mu_3^{MC} - \Delta m_0^{MC}, \sigma_3^{MC}(1 + \epsilon)\right) \right]
$$
$$
+ f_{NG}^{MC} S_{NG}(\Delta m; q^{MC}, \alpha^{MC}), \tag{7}
$$

and $\mathcal{B}$ is the background function

$$
\mathcal{B}(\Delta m) = \Delta m\ \sqrt{u}\ e^{cu}, \tag{8}
$$

where $u \equiv (\Delta m / \Delta m_{\text{thres}})^2 - 1$. The nominal RBW function pole position is located at $m = \Delta m_0 + m(D^0)$ and has natural line width Γ. The Gaussian resolution functions convolved with the RBW have centers offset from zero by small amounts determined from MC, $\mu_i - \Delta m_0^{MC}$. The widths determined from MC, σ_i^{MC}, are scaled by $(1 + \epsilon)$ where ϵ is a common, empirically determined constant which accounts for possible differences between resolutions in data and simulation. The validation of the fit procedure is discussed in Sec. .

Figure 3 shows the fits to data for both D^0 decay modes. The total PDF is shown as the solid curve, the convolved RBW-Gaussian signal as the dashed curve, and the threshold background as the dotted curve. The normalized residuals show the good agreement between the data and the model. Table II summarizes the results of the fits to data for the two modes. The table also shows the fitted S/B at the peak and in the Δm tail on the high side of the peak. The long non-Gaussian tail of the RBW is required for the model to fit the data so well.

SYSTEMATIC UNCERTAINTIES

We have measured the pole mass and the width of the D^{*+} meson with unprecedented precision, analyzing a high-purity sample of continuum produced D^{*+} in $e^+ e^-$ collisions at approximately $10.6\,\text{GeV}$, equivalent to approximately $477\,\text{fb}^{-1}$, collected by the *BABAR* detector. The results for the two independent D^0 decay modes agree with each other well. The dominant systematic uncertainty on the RBW pole position comes from the azimuthal variation. For the decay mode $D^0 \to K^- \pi^+$ we obtain $\Gamma = (83.4 \pm 1.7 \pm 1.5)$ keV and $\Delta m_0 =$

TABLE II. Summary of the results from the fits to data for the $D^0 \to K^- \pi^+$ and $D^0 \to K^- \pi^+ \pi^- \pi^+$ channels (statistical uncertainties only); S/B is the ratio of the convolved signal PDF to the background PDF at the given value of Δm, and ν is the number of degrees of freedom.

Parameter	$D^0 \to K\pi$	$D^0 \to K\pi\pi\pi$
Number of signal events	$138\,539 \pm 109$	$174\,286 \pm 150$
Γ (keV)	83.5 ± 1.7	83.2 ± 1.5
scale factor, $(1 + \epsilon)$	1.06 ± 0.01	1.08 ± 0.01
Δm_0 (keV)	$145\,425.6 \pm 0.6$	$145\,426.6 \pm 0.5$
S/B at peak ($\Delta m = 0.14542\,(\text{GeV})$)	2700	1130
S/B at tail ($\Delta m = 0.1554\,(\text{GeV})$)	0.8	0.3
χ^2/ν	$574/535$	$556/535$

$(145\,425.6 \pm 0.6 \pm 1.8)$ keV while for the decay mode $D^0 \to K^- \pi^+ \pi^- \pi^+$ we obtain $\Gamma = (83.2 \pm 1.5 \pm 2.6)$ keV and $\Delta m_0 = (145\,426.6 \pm 0.5 \pm 2.0)$ keV. Accounting for correlations, we obtain the combined measurement values $\Gamma = (83.3 \pm 1.3 \pm 1.4)$ keV and $\Delta m_0 = (145\,425.8 \pm 0.5 \pm 1.8)$ keV.

We divide the data into disjoint subsets corresponding to intervals of laboratory momentum p of the D^{*+}, azimuthal angle ϕ of the D^{*+} in the laboratory frame, and reconstructed D^0 mass, to search for variations greater than those expected from statistical fluctuations. We also vary the resolution shapes according to their uncertainties and correlations, and estimate uncertainties related to our choice of end point for the fit, the nominal interval size, and the radius assumed in the Blatt-Weisskopf form factor. Finally, we assess systematic uncertainties associated with possible biases observed in fits to MC validation samples. All these uncertainties are estimated independently for the $D^0 \to K^- \pi^+$ and $D^0 \to K^- \pi^+ \pi^- \pi^+$ modes, and are summarized in Table III.

After the corrections to the material model and magnetic field, the laboratory momentum dependence of the RBW pole position is all but eliminated. We find that Γ does not display an azimuthal dependence, however Δm_0 does. Neither Γ nor Δm_0 displays a systematic variation with reconstructed D^0 mass. We discuss in the next subsection how we estimate systematic uncertainties using disjoint subsets.

Systematics using disjoint subsets

We chose to carefully study laboratory momentum, reconstructed D^0 mass, and azimuthal angle ϕ in order to search for variations larger than those expected from statistical fluctuations. For each disjoint subset, we use the resolution function parameter values and Δm_0 offset de-

termined from the corresponding MC subset.

If the fit results from the disjoint subsets are compatible with a constant value, in the sense that $\chi^2/\nu \leq 1$, we assign no systematic uncertainty. However, if we find $\chi^2/\nu > 1$ and do not determine an underlying model which might be used to correct the data, we ascribe an uncertainty using a variation on the scale factor method used by the Particle Data Group (see the discussion of unconstrained averaging [17]). The only sample which we do not fit to a constant is that for Δm_0 in intervals of azimuthal angle. We discuss below how we estimate the associated systematic uncertainty.

In our version of this procedure, we determine a factor that scales the statistical uncertainty to the total uncertainty. The remaining uncertainty is ascribed to unknown detector issues and is used as a measure of systematic uncertainty according to

$$\sigma_{\text{sys}} = \sigma_{\text{stat}} \sqrt{S^2 - 1} \qquad (9)$$

where the scale factor is defined as $S^2 = \chi^2/\nu$. The χ^2 statistic gives a measure of fluctuations, including those expected from statistics, and those from systematic effects. Once we remove the uncertainty expected from statistical fluctuations, we associate what remains with a possible systematic uncertainty.

We expect that χ^2/ν will have an average value of unity if there are no systematic uncertainties that distinguish one subset from another. If systematic deviations from one subset to another exist, then we expect that χ^2/ν will be greater than unity. Even if there are no systematic variations from one disjoint subset to another, χ^2/ν will randomly fluctuate above 1 about half of the time. To be conservative, we assume that any observation of $\chi^2/\nu > 1$ originates from a systematic variation from one disjoint subset to another. This approach has two weaknesses. If used with a large number of subsets it could hide real systematic uncertainties. For example, if instead of 10 subsets we chose 1000 subsets, the larger statistical uncertainties wash out any real systematic variation. Also, if used with a large number of variables, about half the disjoint sets will have upward statistical fluctuations, even in the absence of any systematic variation. We have chosen to use only three disjoint sets of events, and have divided each into 10 subsets to mitigate the effects of such problems.

We chose the range for each subset to have approximately equal statistical sensitivity. In Figs. 4(a) and 4(b) we show the fit results in subsets of laboratory momentum for Γ and Δm_0, respectively. Neither D^0 mode displays a systematic variation; however, we assign small uncertainties for each channel using Eq. (9). Similarly, Figs. 4(c) and 4(d) show the results in ranges of reconstructed D^0 mass for Γ and Δm_0. While neither mode displays a systematic dependence, the width for

TABLE III. Summary of systematic uncertainties with correlation, ρ, between the $D^0 \to K^-\pi^+$ and $D^0 \to K^-\pi^+\pi^-\pi^+$ modes. The $K^-\pi^+$ and $K^-\pi^+\pi^-\pi^+$ invariant masses are denoted by $m\left(D_{\mathrm{reco}}^0\right)$. The methods used to calculate or define the correlations are described in Sec. . The total systematic uncertainties are calculated according to the procedure defined in Sec. .

Source	$\sigma_{sys}\left(\Gamma\right)$ [keV]		ρ	$\sigma_{sys}\left(\Delta m_0\right)$ [keV]		ρ
	$K\pi$	$K\pi\pi\pi$		$K\pi$	$K\pi\pi\pi$	
p dependence	0.88	0.98	0.47	0.24	0.20	0.28
$m\left(D_{\mathrm{reco}}^0\right)$ dependence	0.00	1.53	0.56	0.04	0.00	0.22
Azimuthal dependence	0.62	0.92	-0.04	1.65	1.81	0.84
Magnetic field and material model	0.29	0.18	0.98	0.75	0.81	0.99
Blatt-Weisskopf radius	0.04	0.04	0.99	0.00	0.00	1.00
Variation of resolution shape parameters	0.41	0.37	0.00	0.17	0.16	0.00
Δm fit range	0.83	0.38	-0.42	0.08	0.04	0.35
Background shape near threshold	0.10	0.33	1.00	0.00	0.00	0.00
Interval width for fit	0.00	0.05	0.99	0.00	0.00	0.00
Bias from validation	0.00	1.50	0.00	0.00	0.00	0.00
Radiative effects	0.25	0.11	0.00	0.00	0.00	0.00
Total	1.5	2.6		1.8	2.0	

the $K^-\pi^+\pi^-\pi^+$ mode is assigned its largest uncertainty of 1.53 keV using Eq. (9).

In this analysis we observe sinusoidal variations in the mass values for $D^0 \to K^-\pi^+$, $D^0 \to K^-\pi^+\pi^-\pi^+$, and $K_S^0 \to \pi^+\pi^-$. An extensive investigation revealed that this dependence most probably results from small deviations in the magnetic field from the map used in track reconstruction. For example, if during the field mapping (see Ref. [14]) the propeller arm on which the probes were mounted flexed then the radial and angular components of the magnetic field would have mixed. The important aspect for this analysis is that, for such deviations, the average value is unbiased by the azimuthal variation as evidenced by the corresponding behavior of the K_S^0 mass value. Figures 4(e) and 4(f) show Γ and Δm_0, respectively, in subsets of azimuthal angle. The width does not display a dependence, but each mode is assigned a small uncertainty using Eq. (9). The lack of systematic variation of Γ with respect to ϕ is notable because Δm_0 (which uses reconstructed D masses) shows a clear dependence such that the results for the $D^0 \to K^-\pi^+$ and $D^0 \to K^-\pi^+\pi^-\pi^+$ datasets are highly correlated, and shift together. The signs and phases of these variations agree with those observed for $D^0 \to K^-\pi^+$, $D^0 \to K^-\pi^+\pi^-\pi^+$, and $K_S^0 \to \pi^+\pi^-$. We take half of the amplitude obtained from a sinusoidal fit as a conservative estimate of the uncertainty.

Additional systematics

We assess the uncertainty associated with the correction parameters for the detector material model and magnetic field by examining the variation between the nominal parameter values and those obtained by tuning to the $m_{\mathrm{PDG}}\left(K_S^0\right) \pm 1\sigma_{\mathrm{PDG}}$ mass values [17]. The width mea-

sured from the $D^0 \to K^-\pi^+$ mode fluctuates equally around the value from the fit using the nominal correction parameters. We take the larger of the differences and assign an uncertainty of 0.29 keV. The value of Δm_0 for this mode fluctuates symmetrically around the nominal value and we assign an uncertainty of 0.75 keV. The width measured from the $D^0 \to K^-\pi^+\pi^-\pi^+$ fluctuates asymmetrically around the nominal value, and we use the larger difference to assign an uncertainty of 0.18 keV. The value of Δm_0 for this mode fluctuates symmetrically around the nominal value, and we assign an uncertainty of 0.81 keV.

We use the Blatt-Weisskopf radius $r = 1.6\,\mathrm{GeV}^{-1}$ ($\sim$ 0.3 fm) [13]. To estimate the systematic effect due to the choice of r we refit the distributions treating the D^{*+} as a point-like particle ($r = 0$). We see a small shift of Γ, that we take as the estimate of the uncertainty, and an effect on the RBW pole position that is a factor of 100 smaller than the fit uncertainty, that we neglect.

We determine the systematic uncertainty associated with the resolution function by refitting the data with variations of its parametrization. We take the covariance matrix from the fit to MC resolution samples for each mode and use it to generate 100 variations of these correlated Gaussian-distributed shape parameters. We use these generated values to refit the data, and take the root-mean-squared (RMS) deviation of the resulting fit values as a measure of systematic uncertainty. This process implicitly accounts for the uncertainty associated with the reconstruction offset.

Our choice of fit range is somewhat arbitrary, and so we study the effect of systematically varying its endpoint. This changes the events associated to the RBW tails and those associated to the continuum background. This effectively estimates the uncertainty in the background parameterization. We expect that the larger the Δm fit
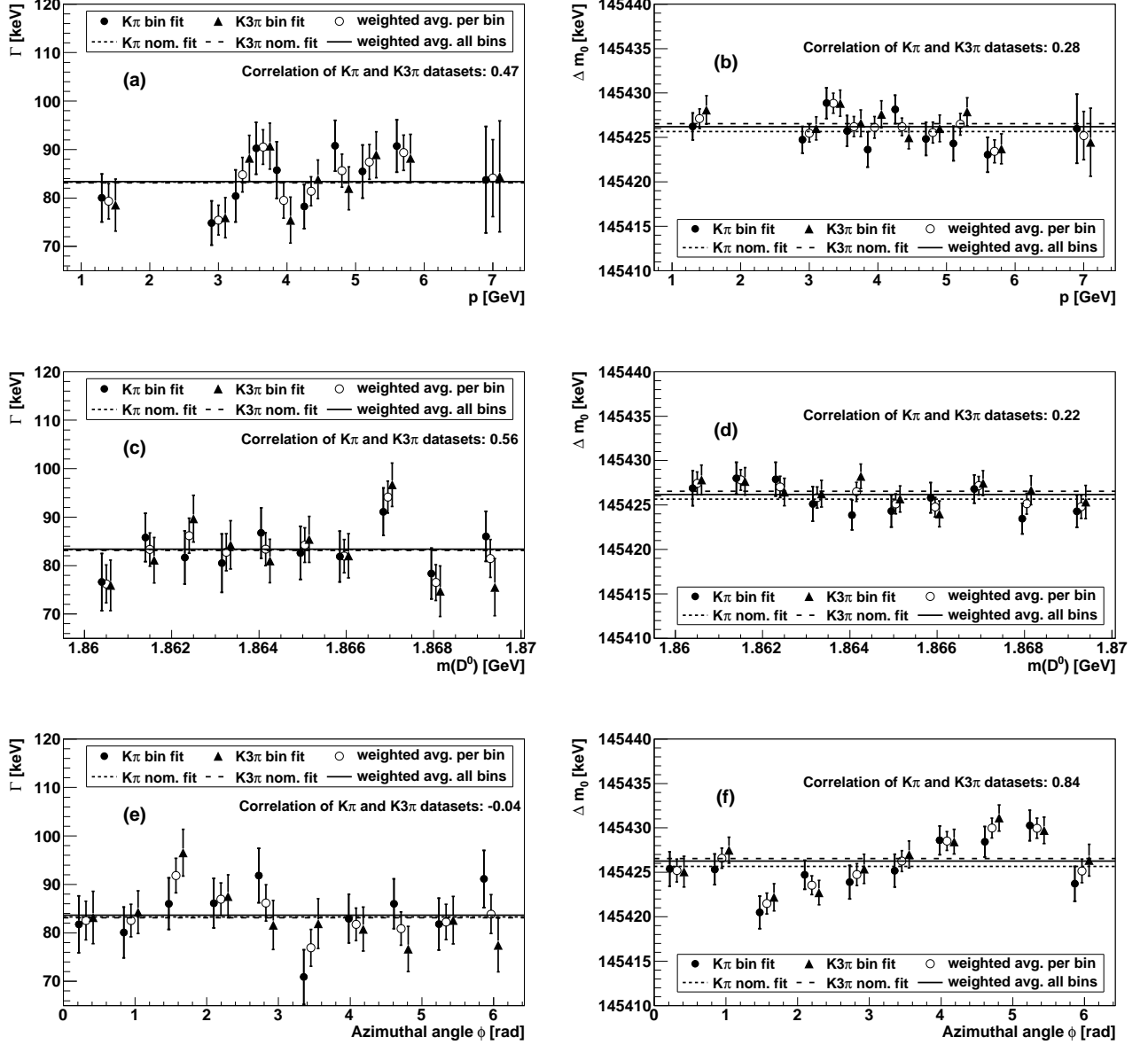
FIG. 4. The values of Γ (left) and Δm_0 (right) obtained from fits to data divided into 10 disjoint subsets in laboratory momentum p (top row), reconstructed D^0 mass (center row), and azimuthal angle (bottom row). The quantities p and ϕ are defined by the D^{*+} momentum. Each point represents an individual fit and each horizontal line is the nominal fit result (i.e. integrating over the variable). The correlation value of Γ (or Δm_0) measured from the $D^0 \to K^-\pi^+$ and $D^0 \to K^-\pi^+\pi^-\pi^+$ samples for each of the variables chosen is given above each plot. The widths from the nominal fits and the weighted average agree well and the corresponding lines are visually indistinguishable.

range, the better description we will obtain for the background and, thereby, a better description of the RBW tails. We vary the end point anyway and take $1\,\mathrm{MeV}$ steps from the nominal fit end point of $\Delta m = 0.1665\,\mathrm{GeV}$ down to $\Delta m = 0.16\,\mathrm{GeV}$. Values below $\Delta m = 0.16\,\mathrm{GeV}$ are too close to the signal region to provide a reasonable choice of end point. There is no clear way to estimate the associated systematic uncertainty, and so we take the largest deviation from the nominal fit as a conservative estimate of the uncertainty.

The shape of the background function in Eq. (8) is nominally determined by only the parameter c and the residuals in Figs. 3(a) and 3(b) show signs of curvature indicating possible systematic problems with the fits. Changing the end points over the range considered changes the values of c substantially from -1.97 to -3.57, and some fits remove all hints of curvature in the residuals plot. We also examine the influence of the background parametrization near threshold by varying the square root in Eq. (8) from 0.5 to nearby values 0.45 and 0.55. The value of the fractional power controls the shape of the background between the signal peak and threshold. For example, at $\Delta m = 0.142$ GeV changing the power from 0.5 to 0.45 and 0.55 varies the background function by $+18\%$ and -15%, respectively. The RBW pole position is unaffected by changing the background description near threshold while Γ shifts symmetrically around its nominal values. We estimate the uncertainty due to the description of the background function near threshold by taking the average difference to the nominal result.

In the binned maximum likelihood fits we nominally choose an interval width of $50\,\mathrm{keV}$. As a systematic check, the interval width was halved and the fits to the data were repeated. The measured Γ and Δm_0 values for both modes are identical except for the width measured in the $D^0 \to K^-\pi^+\pi^-\pi^+$ decay mode. We take the full difference as the systematic uncertainty for the choice of interval width.

Validation samples

We generate signal MC with $\Gamma = 88\,\mathrm{keV}$ and $\Delta m_0 = 0.1454\,\mathrm{GeV}$. The background is taken from a MC cocktail and paired with the signal in the same ratio as from the corresponding fits to data. Fits to both decay modes describe the validation samples well. The fit results are summarized in Table IV. We observe a small bias in the fitted width for the $D^0 \to K^-\pi^+\pi^-\pi^+$ mode. To be conservative, we take the full difference between the fitted and generated value of the width and assign a $1.5\,\mathrm{keV}$ error.

We also investigated the uncertainty due to radiative effects by examining the subset of these events generated without PHOTOS [19]. The values of the RBW pole are

identical between the fits to the total validation signal MC sample and the subsets, so we do not assign a systematic uncertainty to the poles for radiative effects. The widths measured in each mode show a small difference to the results from the nominal validation sample. We take half of this difference as a conservative estimate of the systematic uncertainty associated with radiative effects.

TABLE IV. Summary of results of the fits to the $D^0 \to K^-\pi^+$ and $D^0 \to K^-\pi^+\pi^-\pi^+$ validation MC samples. The width from the $D^0 \to K^-\pi^+\pi^-\pi^+$ decay mode has a small bias, which we take as a systematic uncertainty.

Fit value	Generated	$D^0 \to K\pi$	$D^0 \to K\pi\pi\pi$
$\Gamma\,[\,\mathrm{keV}]$	88.0	88.5 ± 0.8	89.5 ± 0.6
scale factor, $1 + \epsilon$	1.0	1.003 ± 0.004	1.000 ± 0.001
$\Delta m_0\,[\,\mathrm{keV}]$	145400.0	145399.7 ± 0.4	145399.2 ± 0.4
χ^2/ν	–	$613/540$	$770/540$

Determining correlations

The fourth and seventh columns in Table III list the correlations between the $D^0 \to K^-\pi^+$ and $D^0 \to K^-\pi^+\pi^-\pi^+$ systematic uncertainties. These correlations are required to use information from both measurements to compute the average. The correlations in laboratory momentum, reconstructed D^0 mass, and azimuthal angle disjoint subsets are calculated by finding the correlation between the 10 subsets of $D^0 \to K^-\pi^+$ and $D^0 \to K^-\pi^+\pi^-\pi^+$ for each of the variables. In a similar way we can construct datasets using the sets of correction parameters for magnetic field, detector material model, and the Δm fit range. We assume no correlation for the resolution shape parameters and the validation shifts, which are based on the individual reconstructions. Our studies show that the values chosen for the Blatt-Weisskopf radius and interval width affect each mode identically, so we assume that they are completely correlated.

Consistency checks

In addition to the investigations into the sources of systematic uncertainty, we also perform a number of consistency checks. These checks are not used to assess systematics, nor are they included in the final measurements, but serve to reassure us that the experimental approach and fitting technique behave in reasonable ways. First, we lower the p^* cut from $3.6\,\mathrm{GeV}$ to $2.4\,\mathrm{GeV}$. This allows in more background and tracks with poorer resolution, but the statistics increase by a factor of three. Correspondingly, the signal-to-background ratios measured at

the peak and in the tails decrease by approximately a factor of three. The fit results for this larger dataset are consistent with the nominal fit results. The second consistency check widens the reconstructed D^0 mass window from 10 MeV to 30 MeV. Again, this increases the number of background events and improves statistical precision with central values that overlap with the nominal fit results. Finally, we fix the scale factor in the fit to data to report statistical uncertainties on Γ similar to those in the measurement by CLEO [9]. Our reported "statistical" uncertainties on Γ are from a fit in which ϵ floats. As expected, there is a strong negative correlation between ϵ and Γ with $\rho\left(\Gamma,\epsilon\right) \approx -0.85$. If less of the spread in the data is allotted to the resolution function then it must be allotted to the RBW width, Γ. We refit the $D^0 \to K^-\pi^+$ and $D^0 \to K^-\pi^+\pi^-\pi^+$ samples fixing ϵ to the value from the fit where it was allowed to float. This effectively maintains the same global minimum while decoupling the uncertainty in Γ from ϵ. The statistical uncertainty on the width decreases from 1.7 keV to 0.9 keV for the $D^0 \to K^-\pi^+$ decay mode and from 1.5 keV to 0.8 keV for the $D^0 \to K^-\pi^+\pi^-\pi^+$ decay mode.

COMBINING RESULTS

Using the correlations shown in Table III and the formalism briefly outlined below, we determine the values for the combined measurement. For each quantity, Γ and Δm_0, we have a measurement from the $D^0 \to K^-\pi^+$ and $D^0 \to K^-\pi^+\pi^-\pi^+$ modes. So, we start with a 2×2 covariance matrix

$$
V = \begin{pmatrix} \sigma_{K\pi}^2 & \text{cov}(K\pi, K\pi\pi\pi) \\ \text{cov}(K\pi, K\pi\pi\pi) & \sigma_{K\pi\pi\pi}^2 \end{pmatrix}
$$
$$
= \begin{pmatrix} \sigma_{K\pi,\text{stat}}^2 + \sigma_{K\pi,\text{sys}}^2 & \sum_i \rho_i\, \sigma_{K\pi,i}\, \sigma_{K\pi\pi\pi,i} \\ \sum_i \rho_i\, \sigma_{K\pi,i}\, \sigma_{K\pi\pi\pi,i} & \sigma_{K\pi\pi\pi,\text{stat}}^2 + \sigma_{K\pi\pi\pi,\text{sys}}^2 \end{pmatrix} \tag{10}
$$

where i is an index which runs over the sources of systematic uncertainty. In the final step we expand the notation to explicitly show that the diagonal entries incorporate the full systematic uncertainty and that the statistical uncertainty for the individual measurements plays a part in determining the weights. The covariance matrices are calculated using Table III and the individual measurements. From the covariance matrix we extract the weights, w, for the best estimator of the mean and variance using $w_i = \sum_k V_{ik}^{-1} / \sum_{jk} V_{jk}^{-1}$:

$$
w_\Gamma = \begin{pmatrix} w_{K\pi} \\ w_{K\pi\pi\pi} \end{pmatrix} = \begin{pmatrix} 0.648 \\ 0.351 \end{pmatrix} \tag{11}
$$

$$
w_{\Delta m_0} = \begin{pmatrix} w_{K\pi} \\ w_{K\pi\pi\pi} \end{pmatrix} = \begin{pmatrix} 0.647 \\ 0.353 \end{pmatrix}. \tag{12}
$$

The weights show that the combined measurement is dominated by the cleaner $D^0 \to K^-\pi^+$ mode. The total uncertainty can be expressed as

$$
\sigma^2 = \sum_{i=1,2} \left(w_i \sigma_{\text{stat},i}\right)^2
$$
$$
+ \sum_{i=1,2} \left(w_i \sigma_{\text{sys},i}\right)^2 + 2 w_1 w_2 \sum_{j=1,11} \rho_j \sigma_{\text{sys},j}^{K\pi} \sigma_{\text{sys},j}^{K\pi\pi\pi}. \tag{13}
$$

The statistical contribution is the first term and is simply calculated using the individual measurements and the weights. The remaining two terms represent the systematic uncertainty, which is simply the remainder of the total uncertainty after the statistical contribution has been subtracted. The weighted results are $\Gamma = (83.3 \pm 1.3 \pm 1.4)$ keV and $\Delta m_0 = (145\,425.8 \pm 0.5 \pm 1.8)$ keV.

SUMMARY AND CONCLUSIONS

We have measured the pole mass and the width of the D^{*+} meson with unprecedented precision, analyzing a high-purity sample of continuum-produced D^{*+} in e^+e^- collisions at approximately 10.6 GeV, equivalent to approximately 477 fb^{-1}, collected by the *BABAR* detector. The results for the two independent D^0 decay modes agree with each other well. The dominant systematic uncertainty on the RBW pole position comes from the azimuthal variation. For the decay mode $D^0 \to K^-\pi^+$ we obtain $\Gamma = (83.4 \pm 1.7 \pm 1.5)$ keV and $\Delta m_0 = (145\,425.6 \pm 0.6 \pm 1.8)$ keV while for the decay mode $D^0 \to K^-\pi^+\pi^-\pi^+$ we obtain $\Gamma = (83.2 \pm 1.5 \pm 2.6)$ keV and $\Delta m_0 = (145\,426.6 \pm 0.5 \pm 2.0)$ keV. Accounting for correlations, we obtain the combined measurement values $\Gamma = (83.3 \pm 1.3 \pm 1.4)$ keV and $\Delta m_0 = (145\,425.8 \pm 0.5 \pm 1.8)$ keV.

The experimental value of $g_{D^*D\pi}$ is calculated using the relationship between the width and the coupling constant,

$$
\Gamma = \Gamma\left(D^0\pi^+\right) + \Gamma\left(D^+\pi^0\right) + \Gamma\left(D^+\gamma\right) \tag{14}
$$
$$
\approx \Gamma\left(D^0\pi^+\right) + \Gamma\left(D^+\pi^0\right) \tag{15}
$$
$$
\approx \frac{g_{D^*D^0\pi^+}^2}{24\pi m_{D^*+}^2} p_{\pi^+}^3 + \frac{g_{D^*D^+\pi^0}^2}{24\pi m_{D^*+}^2} p_{\pi^0}^3 \tag{16}
$$

where we have again ignored the electromagnetic contribution. The strong couplings can be related through isospin by $g_{D^*D^0\pi^+} = -\sqrt{2}g_{D^*D^+\pi^0}$ [9]. Using Γ and the mass values from Ref. [17] we determine the experimental coupling $g_{D^*D^0\pi^+}^{\text{exp}} = 16.92 \pm 0.13 \pm 0.14$. The universal coupling is directly related to the strong coupling by $\hat{g} = g_{D^*D^0\pi^+} f_\pi / \left(2\sqrt{m_D m_{D^*}}\right)$. This parametrization is

TABLE V. Selected rows from Table 11 of Ref. [21]. State names correspond to the current PDG listings. The third column is the ratio, $R = \Gamma/\hat{g}^2$, extracted from the model in Ref. [21]. The values of $\hat{g}$ were obtained from the data available in 2001.

State	Width (Γ)	R (model)	$\hat{g}$
$D^*(2010)^+$	$96 \pm 4 \pm 22\,\text{keV}$	$143\,\text{keV}$	0.82 ± 0.09
$D_1(2420)^0$	$18.9^{+4.6}_{-3.5}\,\text{MeV}$	$16\,\text{MeV}$	$1.09^{+0.12}_{-0.11}$
$D_2^*(2460)^0$	$23 \pm 5\,\text{MeV}$	$38\,\text{MeV}$	0.77 ± 0.08

TABLE VI. Updated coupling constant values using the latest width measurements. Ratio values are taken from Table V. Significant differences are seen among the coupling constants calculated using the updated width measurements.

State	Width (Γ)	R (model)	$\hat{g}$
$D^*(2010)^+$	$83.3 \pm 1.3 \pm 1.4\,\text{keV}$	$143\,\text{keV}$	0.76 ± 0.01
$D_1(2420)^0$	$31.4 \pm 0.5 \pm 1.3\,\text{MeV}$	$16\,\text{MeV}$	1.40 ± 0.03
$D_2^*(2460)^0$	$50.5 \pm 0.6 \pm 0.7\,\text{MeV}$	$38\,\text{MeV}$	1.15 ± 0.01

different from that of Ref. [9] and is chosen to match a common choice when using chiral perturbation theory, as in Refs. [4, 20]. With this relation and $f_\pi = 130.41\,\text{MeV}$, we find $\hat{g}^{\text{exp}} = 0.570 \pm 0.004 \pm 0.005$.

The paper by Di Pierro and Eichten [21] quotes results in terms of a ratio, $R = \Gamma/\hat{g}^2$, which involves the width of the particular state and provides a straightforward method for calculating the corresponding value of the universal coupling constant within their model. The coupling constant should then take the same value for the selected $D^{(*)}$ decay channels listed in Table V, which shows the values of the ratio R extracted from the model and the experimental values for Γ, as they were in 2001. At the time of publication, $\hat{g}$ was consistent for all of the modes in Ref. [21]. In 2010, BABAR published much more precise results for the $D_1(2420)^0$ and $D_2^*(2460)^0$ [22]. Using those results, this measurement of Γ, and the ratios from Table V, we calculate new values for the coupling constant $\hat{g}$. Table VI shows the updated results. We estimate the uncertainty on the coupling constant value assuming $\sigma_\Gamma \ll \Gamma$. The updated widths reveal significant differences among the extracted values of $\hat{g}$.

The order of magnitude increase in precision confirms the observed inconsistency between the measured D^{*+} width and the chiral quark model calculation by Di Pierro and Eichten [21]. The precise measurements of the widths presented in Table VI provide solid anchor points for future calculations.

[*] Now at the University of Tabuk, Tabuk 71491, Saudi Arabia
[†] Also with Università di Perugia, Dipartimento di Fisica, Perugia, Italy
[‡] Now at the University of Huddersfield, Huddersfield HD1 3DH, UK
[§] Deceased
[¶] Now at University of South Alabama, Mobile, Alabama 36688, USA
[**] Also with Università di Sassari, Sassari, Italy
[1] D. Becirevic and A. L. Yaouanc, JHEP **03**, 021 (1999).
[2] P. Singer, Acta Phys. Pol. B **30**, 3849 (1999).
[3] D. Guetta and P. Singer, Nucl. Phys. Proc. Suppl. **93**, 134 (2001).
[4] B. El-Bennich, M. A. Ivanov, and C. D. Roberts, Phys. Rev. C **83**, 025205 (2011).
[5] G. Burdman et al., Phys. Rev. D **49**, 2331 (1994).
[6] C. Arnesen et al., Phys. Rev. Lett. **95**, 071802 (2005).
[7] J. Bailey et al., Phys. Rev. D **79**, 054507 (2009).
[8] The use of charge conjugate reactions is implied throughout this paper.
[9] A. Anastassov et al. (CLEO Collaboration), Phys. Rev. D **65**, 032003 (2002).
[10] J. M. Blatt and V. F. Weisskopf, Theoretical Nuclear Physics (John Wiley & Sons, New York, 1952).
[11] F. von Hippel and C. Quigg, Phys. Rev. D **5**, 624 (1972).

[12] H. Albrecht *et al.* (ARGUS Collaboration), Phys. Lett. B **308**, 435 (1993).

[13] A. J. Schwartz (for the E791 Collaboration), arXiv:hep-ex/0212057. Contribution to the 5th International Conference Quark Confinement and the Hadron Spectrum, Gargnano (2004).

[14] B. Aubert *et al.* (*BABAR* Collaboration), Nucl. Instr. Methods Phys. Res., Sect. A **479**, 1 (2002).

[15] R. Feynman, *Photon-hadron Interactions* (W. A. Benjamin, Reading, 1972).

[16] B. Aubert *et al.* (*BABAR* Collaboration), Phys. Rev. D **72**, 052006 (2005).

[17] J. Beringer *et al.* (Particle Data Group), Phys. Rev. D **86**, 010001 (2012).

[18] S. Agostinelli *et al.* (Geant4 Collaboration), Nucl. Instr. Methods Phys. Res., Sect. A **506**, 250 (2003).

[19] E. Barberio and Z. Was, Comput. Phys. Commun. **79**, 291 (1994).

[20] A. Abada *et al.*, Phys. Rev. D **66**, 074504 (2002).

[21] M. Di Pierro and E. Eichten, Phys. Rev. D **64**, 114004 (2001).

[22] P. del Amo Sanchez *et al.* (*BABAR* Collaboration), Phys. Rev. D **82**, 111101(R) (2010).